Inorganic Chemistry

Article

pubs.acs.org/IC

Cytotoxicity of Pyrazine-Based Cyclometalated (C^N^{pz}^C)Au(III) Carbene Complexes: Impact of the Nature of the Ancillary Ligand on the Biological Properties

Benoît Bertrand,*[,†] Julio Fernandez-Cestau,[†] Jesus Angulo,[‡] Marco M. D. Cominetti,[‡] Zoë A. E. Waller,[‡] Mark Searcey,[†,‡] Maria A. O'Connell,*[,‡] and Manfred Bochmann*[,†]

[†]School of Chemistry, University of East Anglia, Norwich NR4 7TJ, United Kingdom

[‡]School of Pharmacy, University of East Anglia, Norwich NR4 7TJ, United Kingdom

Supporting Information

ABSTRACT: The synthesis of a series of cyclometalated gold(III) complexes supported by pyrazine-based (C^N^C)-type pincer ligands is reported, including the crystal structure of a cationic example. The compounds provide a new platform for the study of antiproliferative properties of gold(III) complexes. Seven complexes were tested: the neutral series (C^N^{pz}^C)AuX [X = Cl (**1**), 6-thioguanine (**4**), C≡CPh (**5**), SPh (**6**)] and an ionic series that included the *N*-methyl complex [(C^N^{pzMe}^C)AuCl]BF_4 (**7**) and the N-heterocyclic carbene complexes [(C^N^{pz}^C)AuL]$^+$ with L = 1,3-dimethylbenzimidazol-2-ylidene (**2**) or 1,3,7,9-tetramethylxanthin-8-ylidene (**3**). Tests against human leukemia cells identified **1**, **2**, **3**, and **4** as particularly promising, whereas protecting the noncoordinated N atom on the pyrazine ring by methylation (as in **7**) reduced the cytotoxicity. Complex **2** proved to be the most effective of the entire series against the HL60 leukemia, MCF-7 breast cancer, and A549 lung cancer cell lines, with IC_{50} values down to submicromolar levels, associated with a lower toxicity toward healthy human lung fibroblast cells. The benzimidazolylidene complex **2** accumulated more effectively in human lung cancer cells than its caffeine-based analogue **3** and the gold(III) chloride **1**. Compound **2** proved to be unaffected by glutathione under physiological conditions for periods of up to 6 days and stabilizes the DNA G-quadruplex and i-motif structures; the latter is the first such report for gold compounds. We also show the first evidence of inhibition of MDM2−p53 protein−protein interactions by a gold-based compound and identified the binding mode of the compound with MDM2 using saturation transfer difference NMR spectroscopy combined with docking calculations.

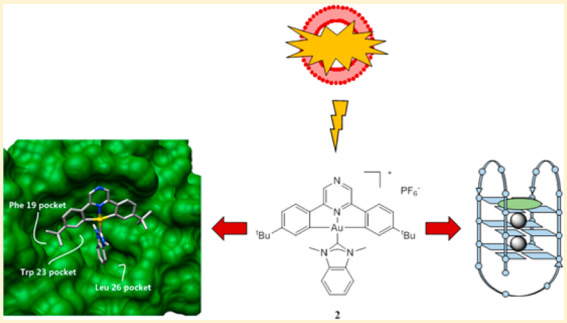

INTRODUCTION

Metallodrugs are widely used for the treatment of several disorders, such as diabetes,[1] rheumatoid arthritis, and cancer.[2] Since the late 1960s, *cis*-diamminedichloroplatinum(II) (cisplatin)[3] has become one of the reference compounds in clinics for the treatment of various types of cancer, including ovarian, testicular, bladder, melanoma, nonsmall cell and small cell lung cancers, lymphomas, and myelomas.[4] However, despite its success, cisplatin presents major drawbacks, such as a limited spectrum of action, acquired resistance to treatment, and severe side effects, which limit the doses administrable to patients.[5] In the search for improvements, many different platinum-based complexes have been synthesized and tested as anticancer drugs in the past decades; however, only two of them (carboplatin and oxaliplatin) have reached worldwide approval.[6] In the quest for new metallodrugs with improved efficacy, a larger spectrum of action, the ability to overcome resistances, and decreased side effects, complexes based on other transition metals have been explored, including Ti,[7] Fe,[8] Cu,[9] Ru,[10] and Au.[11]

Organometallic complexes of gold in the oxidation states +I and +III have proved particularly promising for anticancer purposes.[12] Indeed, complexes bearing N-heterocyclic carbene (NHC) ligands, alkynyl ligands, and cyclometalated arylpyridine ligands are especially efficient in stabilizing Au cations in physiological environments. Special interest has focused in the past few years on cyclometalated complexes in which the Au(III) center is stabilized by (C^N), (C^N^N), or (C^N^C) pincer ligands.[12c,f,13] These complexes also present the advantage of tolerating a large palette of ancillary ligands such as phosphines,[14,15] NHCs,[16] and N-donor ligands,[17,18] enabling optimization of their biological properties. Examples of cyclometalated Au(III) complexes are depicted in Figure 1.

Gold complexes have been reported to often trigger their antiproliferative effects via direct interaction of the Au atom with sulfur or selenium donor atoms of enzymes such as thioredoxin reductase (TrxR),[21] cathepsins,[22] poly(adenosine diphosphate (ADP)-ribose) polymerase 1 (PARP-1),[23] and aquaporins.[24] Che and co-workers[16] showed that although compound **B** (Figure 1) could inhibit cancer cell proliferation

Received: February 7, 2017

DOI: 10.1021/acs.inorgchem.7b00339
Inorg. Chem. XXXX, XXX, XXX−XXX

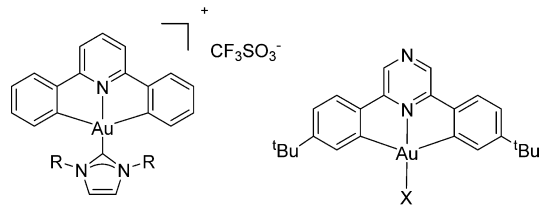

Figure 1. Examples of cyclometalated (C^N^C)Au(III) complexes based on pyridine (**A**, **B**)[15,16] and pyrazine (**C**) ligands[19,20]

at low-submicromolar concentrations, it reacted only poorly with thioredoxin reductase. These authors also reported on the high toxicity, good selectivity, and inhibition of topoisomerase I by complexes of type **A**, a hydrolytically stable cyclometalated Au(III)−NHC complex acting as a structural complex. Although Au complexes have been shown not to interact closely with plasmid DNA,[17] recent reports have demonstrated the ability of organometallic gold(I/III) complexes to stabilize the G-quadruplex structure of DNA.[25] G-quadruplexes are secondary DNA structures formed in guanine-rich sequences by stacking of several G-quartets (cyclic planar assemblies constituted of four guanines maintained around a K^+ cation via a Hoogsteen hydrogen-bonding network).[26] There is good evidence for their occurrence within cell nuclei[27] and for their role in regulating key cellular events, including telomerase activity and oncogene expression.[28] i-Motifs are also DNA secondary structures formed from sequences rich in cytosine and are stabilized by intercalated, hemiprotonated cytosine−cytosine base pairs.[29] i-Motifs have been studied as potential switches in nanotechnology.[30] As i-motif-forming sequences typically oppose regions that can also form G-quadruplexes and stabilization of i-motifs has also been shown to have effects on both telomerase activity and oncogene expression,[31] the selective stabilization of G-quadruplexes or i-motifs is a promising approach for the development of more selective anticancer therapies.[32]

Metal complexes present a broad panel of geometries and oxidation states, features that have been exploited for the design of highly potent and selective metal-based enzyme inhibitors.[33,34] The major strength of those systems is their ability to fit perfectly within the protein site due to the three-dimensional (3D) arrangement of the ligands. The inhibition of protein−protein interactions (PPIs) is emerging as a promising way to treat cancer, and the best inhibitors have entered clinical trials.[35,36] Although most of the PPI inhibitors reported to date are small lipophilic organic molecules, recent reports have shown the potential of octahedral cyclometalated Ir(III) complexes for PPI inhibition.[37,38] Indeed, one of those was shown to disrupt the interactions between tumor necrosis factor α (TNF-α) and tumor necrosis factor receptor (TNFR) more efficiently than the known organic inhibitor SPD304 by fitting more closely within the binding pocket.[38] One of the most studied PPIs is the E3 ubiquitin-protein ligase MDM2−p53 interaction. Indeed, p53 acts as a tumor suppressor and is found to have reduced activity in the majority of cancers. A reason for reduced p53 activity is overexpression of MDM2, which inhibits the p53 activity via PPI, making the disruption of the interaction between MDM2 and p53 a very promising target for the development of selective anticancer therapy.[39] Although some cyclometalated (C^N)Au(III) complexes have been reported to exhibit p53-dependent cytotoxic activity,[14] to the best of our knowledge, no gold-based complexes have yet been reported to disrupt PPIs.

We recently reported the synthesis of a series of 2,6-bis(4′-*tert*-butylphenyl)pyrazine (C^N^{pz}^C)-type Au(III) complexes (Figure 1, structure **C**; X = Cl, C≡CPh, SR).[19,20] The photoluminescence exhibited by these complexes may enable the visualization of the uptake of the compounds and their intracellular distribution by fluorescence microscopy, which is impossible to do with classical pyridine-based pincers. Remarkably, (C^N^{pz}^C)Au(III) complexes are not reduced

Scheme 1. Synthesis of Pyrazine-Based (C^N^{pz}^C)Au(III) Complexes 2−4 and Structures of the Previously Reported Complexes 5−7; The Structure of 1 Shows the Numbering System Used for NMR Assignments

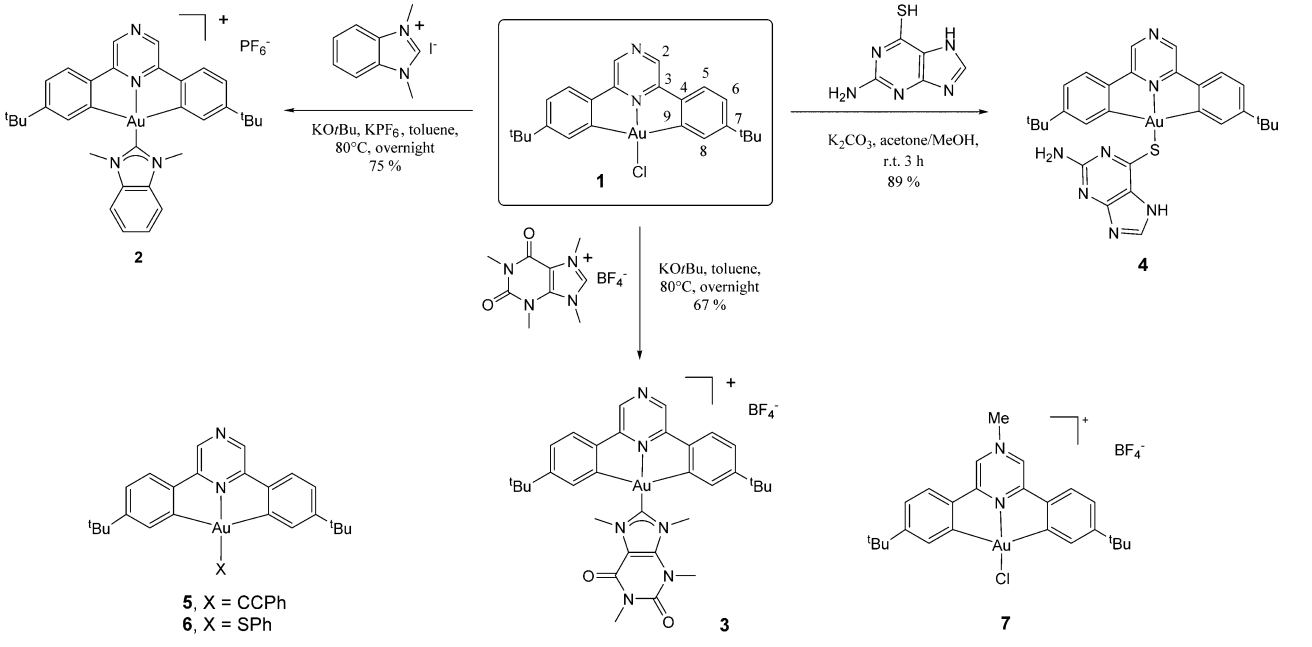

DOI: 10.1021/acs.inorgchem.7b00339
Inorg. Chem. XXXX, XXX, XXX−XXX

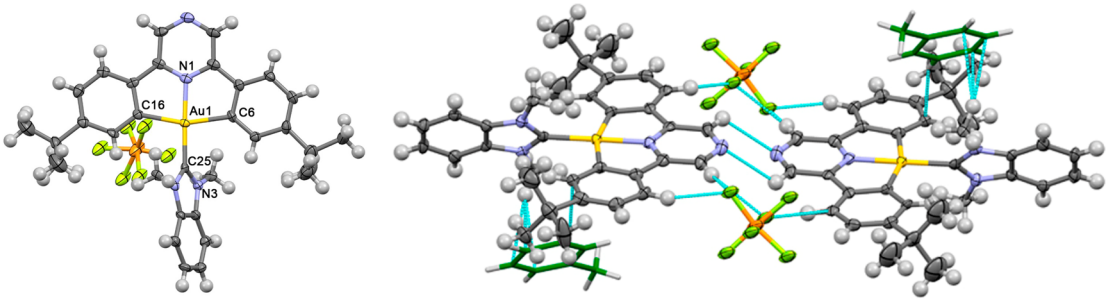

Figure 2. (left) Molecular structure of the cation in **2**·toluene. The atomic numbering scheme is also shown. Selected bond distances [Å] and angles [deg]: Au1−N1 1.991(9), Au1−C25 1.995(10), Au1−C6 2.099(10), Au1−C16 2.096(11), C6−Au1−C25 97.8(4), C16−Au1−C25 100.9(4), torsion angle N1−Au1−C25−N3 125.73. (right) Crystal packing and hydrogen-bonding interactions involving the pyrazine moiety. Color coding: C (gray), Au (yellow), N (blue), P (orange); F (light green); toluene (dark green).

by thiols, and the pyrazine rings in these planar ligands have a tendency for hydrogen bonding as well as π stacking,[20] all of which may be relevant for understanding their biological activity.

We report here the synthesis and characterization of three new cyclometalated (C^N^{pz}^C)Au(III) complexes: two cationic complexes with NHC ligands, i.e., 1,3-dimethylbenzimidazol-2-ylidene (**2**) and 1,3,7,9-tetramethylxanthin-8-ylidene (**3**) (Scheme 1), and a neutral one with the known anticancer agent 6-thioguanine (**4**). Although Au(I) complexes of 1,3,7,9-tetramethylxanthin-8-ylidene and 6-thioguanine are known,[25b,40] this is the first report of the use of these ligands in Au(III) chemistry. These complexes together with compounds **1** and **5**−**7** and the free pincer ligand HC^N^{pz}^CH (**L**) were screened for their antiproliferative properties at concentrations of 10 and 1 μM on HL60 leukemia cells. The IC_{50} values of the best candidates were then measured on the HL60, MCF-7 (breast cancer), and A549 (human adenocarcinoma lung cancer) cell lines as well as on MRC-5 cells (human lung fibroblasts) as a model of healthy cells. The responses were compared with those of cisplatin. The uptake of the compounds into the cells and the interactions with possible intracellular targets were investigated.

RESULTS AND DISCUSSION

Synthesis and Characterization. The reaction of (C^N^{pz}^C)AuCl (**1**) with the *N*,*N*-dimethylbenzimidazolium or xanthinium salts in the presence of potassium *tert*-butoxide gave good yields of the ionic NHC complexes **2** and **3**, respectively (Scheme 1). The formation of the compounds was conveniently monitored by ^{1}H NMR spectroscopy. The conversions of **1** to **2** and **3** were indicated by downfield shifts of the H^8 proton by 0.9 and 0.7 ppm, respectively. The carbene ^{13}C NMR signals for **2** and **3** were observed at $\delta^{13}_{C\{^1H\}}$ = 162.5 and 159.1 ppm, respectively.

The reaction of **1** with 6-thioguanine (6-TG) in the presence of potassium carbonate following reported procedures[14,20] gave the (C^N^{pz}^C)Au(6-TG) (**4**) in good yield. The ^{1}H NMR signal of the H^8 proton appeared at δ^1_H = 7.57 ppm and the ^{13}C NMR signal of the cyclometalated carbon C^9 appeared at $\delta^{13}_{C\{^1H\}}$ = 170.2 ppm, in good agreement with what we obtained for other (C^N^{pz}^C)Au thiolates.[20]

Crystals of **2**·toluene suitable for X-ray diffraction were grown by slow evaporation of a saturated solution in dichloromethane/toluene (9/1). The structure (Figure 2) confirms the distorted square-planar coordination sphere for the Au(III) center. The bond distances lie within the range expected for this type of complex. In particular, the Au1−C25(carbene) distance of 1.995(10) Å in **2**·toluene compares well with those in other gold(III)−carbene complexes (1.967−2.017 Å),[41] In **2**·toluene the carbene ligand is oriented roughly perpendicular to the AuC_2N plane (dihedral angle = 125.73°). The crystal packing shows hydrogen-bonding interactions between pyrazine rings of two neighboring molecules and two PF_6 anions confining this dimerization (Figure 2). The formation of this sort of $\{[(C^N^{pz}^C)Au(NHC)](PF_6)\}_2$ dimer in the crystal lattice contrasts with the supramolecular interactions found in pyridine-based (C^N^C)Au−carbene complexes.[41] As noted in the Introduction, the nature of this sort of interaction is likely to be important to the understanding of the biological activity of the complexes. As the X-ray crystal structure suggests, the type and strength of the intermolecular interactions are driven by the central ring of the cyclometalated ligand.

Although insoluble in purely aqueous media, all of the compounds appeared soluble enough in dimethyl sulfoxide (DMSO) not to precipitate when diluted in aqueous media up to 50 μM with 1% DMSO and up to 100 μM with 10% DMSO.

Photophysical Properties. Theranostics (compounds associating an active drug with an imaging agent) enable tracking of the drug after treatment and thus help elucidate the drug's mode of action.[42] As we reported recently,[19] the photophysical properties of pyrazine-based complexes are dominated by the (C^N^{pz}^C) pincer ligand. On the basis of those findings, we measured the photophysical properties of the newly synthesized complexes (Table 1) to test whether they were emissive enough to be tracked inside the cells. The most relevant absorptions in the UV−vis spectrum are the characteristic low-energy bands attributed to metal-perturbed (C^N^{pz}^C) singlet-state intraligand (^{1}IL) transitions. The intense green luminescence of all of the complexes is due to (C^N^{pz}^C) triplet-state intraligand (^{3}IL) transitions, which

Table 1. Photophysical Data for Complexes 2 and 3 in CH_2Cl_2 Solution at 298 K

complex	λ_{abs}/nm ($10^{-3}\varepsilon$/M^{-1} cm^{-1})	λ_{em}/nm (λ_{ex}/nm)	Φ/%[a]
2	278 (16.7), 321 (10.5), 345 (6.8), 409 (3.1), 430 (4.6), 456 (4.5)	536_{max}, 571_{sh} (300−420)	0.170
3	270 (23.7), 322 (7.34), 352 (5.3), 432 (2.4), 456 (2.3)	536_{max}, 571_{sh} (300−420)	0.170

[a]Relative to $[Ru(bpy)_3]^{2+}$ in H_2O as a standard (Φ_{stn} = 2.8%).

DOI: 10.1021/acs.inorgchem.7b00339
Inorg. Chem. XXXX, XXX, XXX−XXX

show vibronic progression. The smaller energy gap of these transitions in **2** and **3** compared with the pyridine analogues under identical conditions enhances the ligand-to-ligand charge transfer (LLCT) (NHC → C^N^{pz}^C) character of the transitions responsible for the low-energy absorption and the emission. The quantum yields of both complexes are relatively high for gold (C^N^C) pincer compounds in solution. Although (C^N^{pz}^C)Au(III) alkyl and aryl thiolates had previously been found to be luminescent,[20] the thiolate **4** proved not to be emissive in solution at room temperature. This limits the use of luminescence for the visualization of the intracellular uptake and localization of these compounds using fluorescence microscopy.

Antiproliferative Activity in Vitro. An initial screening of compounds **1**−**7** was carried out on human promyelocytic leukemia (HL60) cells. The inhibition of the proliferation of HL60 cells was determined using the established MTS assay (see the Experimental Section) after 72 h of incubation with **1**−**7**, the free pincer ligand (**L**), or cisplatin at a concentration of 10 or 1 μM (Figure 3). All of the gold compounds as well as the free ligand **L** were predissolved in DMSO and then diluted 100-fold in the culture medium containing the cells to reach the final concentration of compound and the nontoxic final DMSO concentration of 1%. Cisplatin was dissolved in water and further diluted 100-fold with the culture medium with cells following the method used for the other compounds.

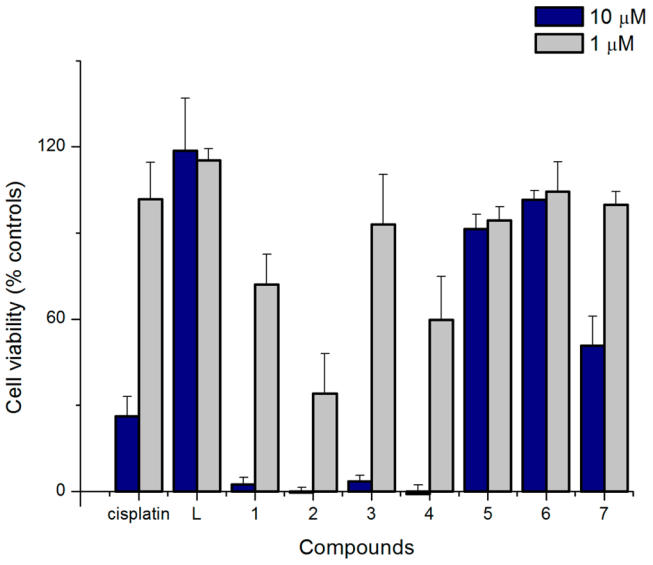

Figure 3. Inhibition of HL60 cell proliferation by (C^N^{pz}^C)Au(III) complexes **1**−**7**; data represent the average ± standard error of three experiments.

At a concentration of 10 μM, the various types of ancillary ligands gave very different cell viability responses. While the compounds containing NHC ligands (**2** and **3**) and the compound bearing the anticancer moiety 6-TG (**4**) completely inhibited cell proliferation, the neutral alkynyl and thiophenolate complexes (**5** and **6**, respectively) were nontoxic. Methylation of the pyrazine N atom, as in compound **7**, strongly reduced the cytotoxicity compared with the non-methylated analogue **1**, which fully inhibited cell growth at the same concentration; the presence or absence of a positive charge on the (C^N^{pz}^C)Au framework is therefore not in itself a decisive factor. As a control, at 10 μM the free 2,6-diarylpyrazine ligand **L** itself did not show any toxic effect.

Reducing the concentration to 1 μM allowed further discrimination. The caffeine-derived NHC complex **3** was nontoxic at that concentration, and compounds **1** and **4** were only moderately active (cell viability of 72% and 60%, respectively), whereas the benzimidazolylidene complex **2** showed strong antiproliferative activity, with the cell viability reduced to 22%.

The four compounds that showed strong cytotoxic effects at a concentration of 10 μM (i.e., **1**−**4**) were selected for the determination of values of IC_{50} (i.e., the concentration required to inhibit 50% of cells from growing) on a panel of human cancer cell lines, including leukemia (HL60), breast adenocarcinoma (MCF-7), and human lung adenocarcinoma (A549) cells and, for comparison with healthy cells, human fetal lung fibroblast (MRC-5) cells. The results are reported in Table 2.

Table 2. Effects of Compounds 1−4, 6-TG, and Cisplatin on Cell Viability in Human Leukemia (HL60), Human Breast Adenocarcinoma (MCF-7), Human Lung Adenocarcinoma Epithelial (A549), and Human Fetal Lung Fibroblast (MRC-5) Cells after 72 h of Incubation

	IC_{50} ± SE (μM)[a]			
compound	HL60	MCF-7	A549	MRC-5
1	3.71 ± 0.29	8.6 ± 1.1	>50	4.9 ± 0.6
2	0.31 ± 0.15	0.56 ± 0.02	7.8 ± 1.3	1.4 ± 0.4
3	4.05 ± 0.43	7.90 ± 0.13	>50	17.6 ± 1.9
4	0.90 ± 0.22	0.78 ± 0.11	29.0 ± 1.8	4.3 ± 0.7
cisplatin	3.70 ± 0.25	21.2 ± 3.9	33.7 ± 3.7	10.7 ± 3.0
6-TG	0.98 ± 0.07	0.42 ± 0.13	>50	>50

[a]Values are reported as IC_{50} ± mean standard error (SE) of three independent experiments.

Compound **2** bearing the benzimidazole-based NHC ligand proved to be the most toxic of the series; its IC_{50} values in the micromolar to submicromolar range were 1 order of magnitude lower against all cancer cell lines than those of complexes **1** and **3** and cisplatin. The exception was the highly resistant A549 cell line, against which **2** was only 4 times more toxic than cisplatin. Despite the close structural similarity between NHC compounds **2** and **3**, there was a dramatic difference in cytotoxic effects, with **2** being up to 14 times more potent than **3** against MCF-7 cells.

The A549 cell line is known to exhibit cisplatin resistance (due to overexpression of DNA repair enzymes such as apurinic/apyrimidinic endonuclease 1 (APE1) or PARP),[43] and we found a decrease in activity for all of the tested compounds against A549 compared with the HL60 and MCF-7 cell lines. However, while compounds **1** and **3** appeared completely nontoxic up to a concentration of 50 μM and compound **4** appeared weakly toxic (IC_{50} = 29.0 ± 1.8 μM) against A549 cells, the activity of **2** was encouragingly high, with an IC_{50} of 7.8 ± 1.3 μM. It appears that the highly polar caffeine-based NHC ligand is very much less effective than the hydrophobic benzimidazolylidene ligand.

It is worth mentioning that although no strict direct comparison with other reported (C^N^C)Au NHC complexes is possible because they were tested against different cell lines, complex **2** presents IC_{50} values in the same low- to submicromolar range as previously reported complexes.[15,16]

DOI: 10.1021/acs.inorgchem.7b00339
Inorg. Chem. XXXX, XXX, XXX−XXX

Compared with related Au(I) NHC complexes, the Au(III) complex **2** turned out to be more than twice as toxic as (benzimidazolylidene)AuCl against A549 cells[25b] and more than 10 times more toxic against MCF-7 cells.[44] Moreover, the toxicities of complex **2** against A549 and MCF-7 cells compare well with those of $[(\text{benzimidazolylidene})_2\text{Au}]^+$.[25b,45] Encouragingly, both **2** and **3** were 2−4 times less toxic toward healthy fibroblasts (MRC-5) than toward the HL60 and MCF-7 cancer cell lines, although of course further improvements in selectivity will be required for the future development of these potential drugs.

Compound **4** was toxic at submicromolar levels against HL60 and MCF-7 cells (IC_{50} = 0.90 ± 0.22 and 0.78 ± 0.11 μM, respectively) and weakly toxic against A549 cells (IC_{50} = 29.0 ± 1.8 μM), following exactly the toxicity pattern of its ligand, 6-TG. While free 6-TG appeared nontoxic against healthy fibroblasts, compound **4** showed toxicity in the low-micromolar range (IC_{50} = 4.3 ± 0.7 μM) and a similar selectivity ratio as compounds **2** and **3**. Compound **6**, the thiophenolate analogue of **4**, was shown to be completely inactive and demonstrates the poor cytotoxicity of the (C^N^{pz}^C)AuS moiety. These data suggest that the cytotoxic properties of **4** might arise predominantly from the 6-TG ligand rather than from the (C^N^{pz}^C)Au scaffold.

Cellular Uptake. Cellular uptake and accumulation are major factors involved in the cytotoxicity of drugs.[46] In order to measure the amount of compound taken up by the cells, we quantified the cellular gold content using inductively coupled plasma mass spectrometry (ICP-MS). We selected for that study the most cytotoxic compound **2**, its caffeine analogue **3**, and the starting chloride **1** to investigate the impact of the NHC ligand and its nature on the cellular uptake. We used the A549 cells, which gave the most important discrimination between nontoxic compounds **1** and **3** and highly cytotoxic **2**, and the MCF-7 cells, which were sensitive to compounds **1**−**3**. Considering the respective IC_{50} values for **2** against A549 and MCF-7 cells, these cell lines were incubated for 6 h with 10 μM and 1 μM solutions of the gold compounds, respectively, as described in the Experimental Section. The results of three independent experiments are depicted in Figure 4 for A549 cells and in Figure S1 for MCF-7 cells.

Remarkably, compound **2** shows a much higher uptake into A549 cells than either **1** or **3**. Indeed, the intracellular gold concentration of **2** was almost 4 and 11 times higher than those of **1** and **3**, respectively, in good agreement with the results of the in vitro screening. The difference between the structurally analogous cationic NHC complexes **2** and **3** is particularly striking. Evidently, the presence of polar functional groups on the caffeine-based NHC ligand of **3** impedes rather than assists the uptake process into cancer cells. Similar behavior was noticed with MCF-7 cells (Figure S1), confirming the deleterious impact of the methylcaffeinylidene ligand on the cell uptake of the (C^N^{pz}^C)Au−NHC scaffold.

Reaction of 2 with Glutathione. Glutathione (GSH) is a tripeptide that is present at millimolar levels inside cells and is overexpressed in most cancer cells. GSH is involved in many different cellular functions, such as xenobiotic detoxification, reactive oxygen species (ROS) scavenging, and cellular redox balance maintenance.[47] GSH has been shown to be involved in the mechanism of cisplatin resistance (a) by reducing the intracellular amount of cisplatin via multidrug resistance protein-2 (MRP-2)-mediated efflux and (b) by acting as a redox-regulating agent.[48] GSH is known to deactivate Au(III) complexes by reduction to Au(I) or Au(0). Reduction by GSH has even been observed in Au(III) complexes bearing (N^N) or (N^N^N) chelating ligands, leading to deactivation of the compounds.[49]

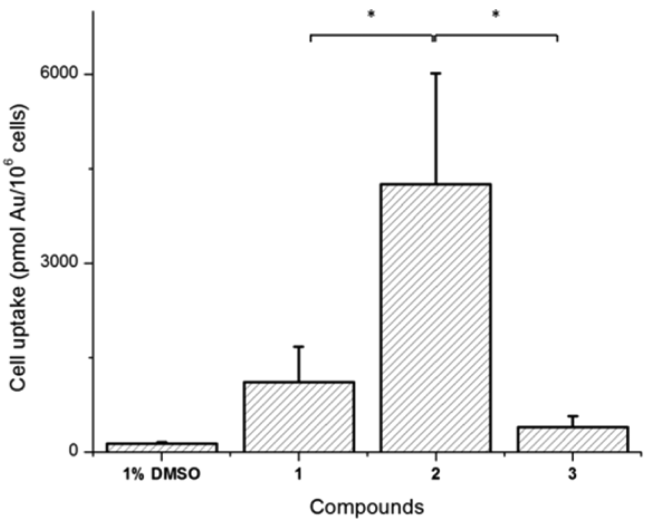

Figure 4. Cell uptake of compounds **1**−**3** by A549 cells after 6 h of treatment with compounds at 10 μM in DMSO. The significance of the results was analyzed by the *t* test: *, $p < 0.05$.

We investigated the reactivity of the most promising compound, **2**, with GSH by ^{1}H NMR spectroscopy by monitoring mixtures of equimolar amounts of **2** and GSH (10 mM) in DMSO-d_6 over a period of 6 days at room temperature, following the procedure described for Pt(IV) complexes.[50] The aromatic regions of the different spectra are presented in Figure S2. Over that period of time there was neither reduction to Au(0) or Au(I) nor the appearance of the signals corresponding to the free ligand, HC^N^{pz}^CH. Evidently, pyrazine-based Au(III) pincer complexes are resistant to reduction by GSH, at least over the duration of the experiment, i.e., the NHC ligand is not substituted during these reactions. As we showed recently, stable (C^N^{pz}^C)AuSR complexes can indeed be isolated under different conditions, but these too are resistant to reduction.[20] Additionally, in contrast to what has been observed by Che et al. on (C^N)- and (N^N^N)Au(III) complexes,[18,49b] no substitution reaction by GSH of either the NHC ligand or one arm of the (C^N^{pz}^C) pincer ligand was observed. Taken together, these data confirm the high stability of **2** toward GSH. The data therefore suggest that **2** is unlikely to trigger its antiproliferative effects via direct coordination of sulfur-donor-containing enzymes like TrxR or PARP-1 as reported for other Au(III) complexes.[14,15,21] Thus, compound **2** might be considered as a structural type that interacts with its targets via supramolecular interactions.

DNA-Binding Properties. G-quadruplexes are secondary structures of DNA formed by stacking of tetrads of guanine residues linked via Hoogsteen hydrogen bonding and stabilized by the presence of typically monovalent cations in the center of the tetrad.[28] The selective stabilization of those structures has been investigated as a means of controlling key cellular events such as telomerase activity and oncogene expression,[29] making the development of G-quadruplex ligands promising anticancer candidates.[33] Recent reports on organometallic Au(I/III) complexes have highlighted the G-quadruplex structure of DNA as a possible intracellular target for these classes of

DOI: 10.1021/acs.inorgchem.7b00339
Inorg. Chem. XXXX, XXX, XXX−XXX

compounds.[25] Recently, a caffeine-based bis(NHC)gold(I) cation has been cocrystallized with a G-quadruplex, showing that the DNA−ligand interaction occurred via π stacking on the accessible tetrads.[25d]

Another possible target for complex−DNA interactions are i-motifs. These are cytosine-rich sequences that can form higher-order structures via hydrogen bonding between hemiprotonated pairs of cytosines.[31] i-Motifs require sequences that have stretches of multiple cytosines and thus are likely to form in the complementary strands opposing G-quadruplexes in the genome. Although they are inherently less stable than G-quadruplexes, the stabilization of i-motifs has been shown to alter gene expression of the oncogene bcl-2 and disrupt telomerase function, therefore also indicating potential as a target for anticancer drugs.[51] Considering that (C^N^C)Au−NHC complexes have been demonstrated to be able to enter the cell nucleus[52] and in view of the structure of our best candidate in the antiproliferative assay (planar with a large π surface and monocationic charge) and the general high stability of our (C^N^{pz}^C)Au(III) complexes toward GSH, we screened the compounds for their potential to bind to DNA G-quadruplex and i-motif structures.

To give a broad indication of the DNA binding capabilities, compounds **1**−**7** were assessed with the established Förster resonance energy transfer (FRET) DNA-melting assay[53] against different DNA targets: the G-quadruplex-forming sequence from the human telomere (hTeloG), the human telomeric i-motif sequence (hTeloC), an i-motif-forming sequence from the promoter region of the oncogene hif-1α, and double-stranded DNA. The i-motif-forming sequence from the human telomere is not stable at neutral pH, so this was assessed at pH 5.5, where the structure is folded, and at the transitional pH 6.0, where it is 50% folded.[54] The remaining sequences were all tested at the transitional pH of hif-1α, pH 7.2.[55]

From that preliminary screening using 50 equiv of compounds (Figure 5), it was evident that both NHC complexes **2** and **3** presented good interactions with both the G-quadruplex and i-motif structures, whereas none of other complexes interacted with any of the tested structures, including double-stranded DNA. Somewhat surprisingly, this was also the case for the cationic *N*-methyl complex **7**, so the presence of charge alone is not responsible for DNA interactions. Moreover, the neutral complex **5** bearing a phenylacetylenyl ligand with an extended π surface did not show any interaction with the studied DNA structures. This suggests that the good interactions of the cationic NHC complexes **2** and **3** may be due to the combination of the cationic charge, the increase in the π surface, and hydrogen bonding to the noncoordinated pyrazine N atom. The neutral compound **4** bearing a thioguanine ligand (of the same nature as the components of G4 tetrads) did not show any interaction with the studied DNA structures, as noticed for its thiophenol analogue **6**.

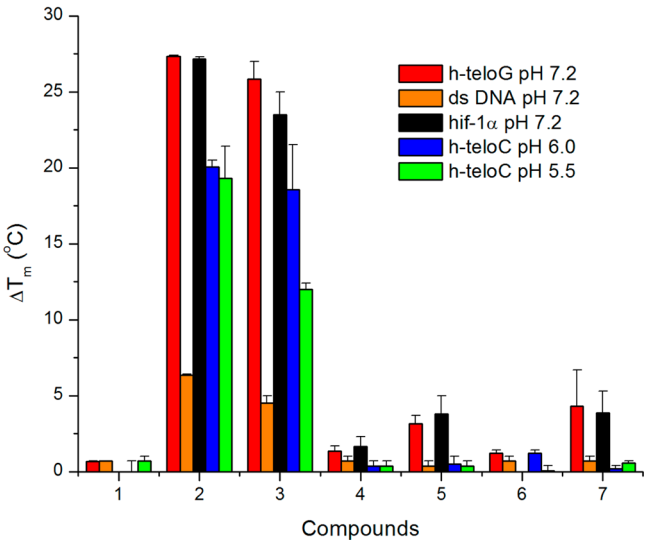

Figure 5. Stabilization of different DNA structures (0.2 μM) by pyrazine-based (C^N^{pz}^C)Au complexes **1**−**7** at 10 μM measured by FRET DNA-melting assay. Data represent the average and standard deviation of three experiments.

Both NHC-based compounds **2** and **3** interact in a dose-dependent manner with all of the DNA structures (see Figures S3 and S4). Compounds **2** and **3** were found to interact more strongly with the human telomeric G-quadruplex sequence (ΔT_m up to 40 and 31 °C at [Au] = 20 μM for **2** and **3**, respectively) than with either the hif-1α i-motif sequence (ΔT_m up to 31 and 24 °C at [Au] = 20 μM for **2** and **3**, respectively) or the human telomeric i-motif sequence.

While **3** does not show any particular difference in its interaction with either the human telomeric i-motif sequence at both pH 5.5 and pH 6.0 or with hif-1α at pH 7.2, **2** seemed to stabilize the telomeric i-motif structure at pH 6.0 more efficiently than at pH 5.5; it also stabilized hif-1α at physiological pH (pH 7.2). To the best of our knowledge, this is the first report of gold complexes stabilizing an i-motif structure of DNA.

Replacing the benzimidazole-based carbene by a caffeine-based one reduced the ability of the compound to interact with classical double-stranded DNA (ΔT_m up to 14 and 7 °C at 20 μM **2** and **3**, respectively), as previously observed in the case of bis(NHC)Au(I) complexes.[25b]

Inhibition of MDM2−p53 Interaction. Considering that both MCF-7 and A549 cells present wild-type p53,[56] the interactions of our compounds with MDM2 and their ability to disrupt the MDM2−p53 interaction were also explored. Compounds **1**−**3** and **5** and the free ligand **L** were screened as potential inhibitors using a fluorescence polarization assay as previously described.[57] Human MDM2 protein (residues 17−125) was used in the polarization assay, and the wild-type p53 peptide (residues 15−27) was used as a positive control. Among the three gold-based complexes and the free ligand screened at a concentration of 100 μM, only compounds **1** and **2** appeared to disrupt the MDM2−p53 interaction, highlighting first the relevance of the gold cation and second the impact of the ancillary ligand. Compounds **1** and **2** were further evaluated to determine their IC_{50} values. The most efficient inhibitor was **2**, with an IC_{50} of 31.1 ± 1.1 μM, while **1** has an IC_{50} of 48.8 ± 3.1 μM.

After the positive fluorescence polarization results, the interaction of compound **2** with MDM2 was confirmed using high-resolution saturation transfer difference NMR spectroscopy (STD NMR).[58] STD NMR has already been demonstrated to be a powerful tool to characterize pharmacophoric information on the binding of ligands to MDM2.[59] In our case, STD NMR experiments clearly confirmed the binding of **2** to MDM2 in solution (Figure 6), in agreement with the fluorescence polarization results. Clear signals were observed in

DOI: 10.1021/acs.inorgchem.7b00339
Inorg. Chem. XXXX, XXX, XXX−XXX

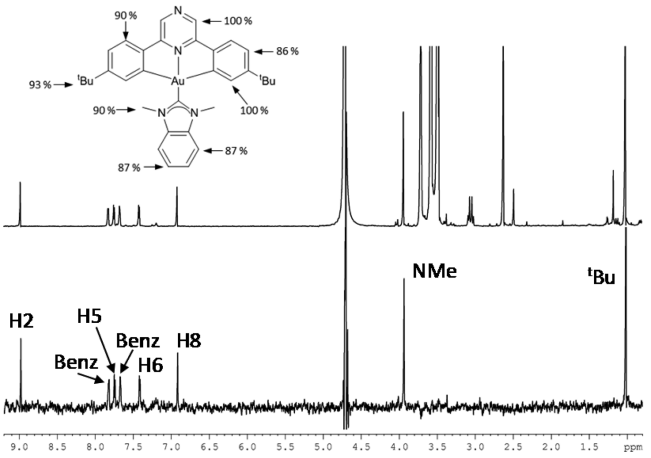

Figure 6. Interaction of **2** with MDM2 in solution studied by STD NMR (13.5 μM MDM2, 500 μM **2**, 1% DMSO-d_6, 800 MHz, 25 °C). (top) ^{1}H NMR reference spectrum. The inset shows the group epitope mapping of **2** from STD NMR experiments derived from STD NMR intensities at very low saturation time (0.5 s). Ligand hydrogens showing high % values have close contacts with the surface of the binding pocket of MDM2. (bottom) STD NMR spectrum (4 s saturation time) showing signals of **2** resulting from the binding in solution (intense signals around 3.5−3.7 ppm in the reference spectrum belong to glycerol, which does not bind to MDM2.

the difference spectrum, arising from the transfer of saturation from the protein, which can only occur in the bound state (Figure 6, bottom). In contrast, glycerol and residual DMSO signals did not appear in the difference spectrum.

From the intensities of the STD NMR experiments we were able to depict the binding epitope of **2** for the interaction with MDM2, mapping in this way the main ligand contacts in the binding pocket of MDM2 (Figure 6 inset). This was done by normalization of all of the STD intensities against the strongest one (Figure 6 inset). As the average deviation of epitope mapping by STD NMR has been previously determined to be around 7%,[60] the values in Figure 6 show a highly homogeneous distribution of normalized STD values (Figure 6 inset), indicating that **2** contacts MDM2 all along its structure in the bound state. In this way, the experimental NMR data support a binding mode in which **2** is almost fully buried in the p53-specific hydrophobic binding pocket of MDM2, which is in agreement with the hydrophobic character of the compound and the typical binding of small ligands to MDM2.

To further investigate the structural details of the binding of **2** to MDM2 and to provide a 3D model of the complex, we carried out docking calculations in a model of MDM2. The interaction between MDM2 and p53 is well-characterized; crystallization of the domains involved and mutagenesis studies have clarified the structures involved and the main features of the interaction.[61] An amphiphilic α-helix near the N-terminus of p53 (amino acids 18−26) interacts with a hydrophobic cleft at the N-terminal domain of MDM2. The most relevant residues of p53 involved in the interaction are Phe19, Trp23, and Leu26, occupying the deep pockets available on the interaction surface of MDM2. A number of synthetic molecules have been shown to take advantage of this binding epitope to inhibit the interaction between MDM2 and p53.[57,62]

According to the results previously described in this paper, direct interaction with methionine residues as main mode of binding was excluded, and focus was given to the docking of the molecule directly into the pockets occupied by p53. The result of the docking calculations of **2** and MDM2 is shown in Figure 7 (for details on the calculations and analysis, see the Experimental Section). Compound **2** sits with the ancillary ligand partially in the pocket occupied by Leu 26 of p53. One of the *tert*-butyl groups lies on the Phe 19 pocket while the opposite one lies near the N-terminus of MDM2. The (C^N^{pz}^C) ligand lies against the α-helix between residues 50 and 63. Such an interaction also obstructs access to the Trp 23 pocket, which is enclosed by the ligand. The interactions are mainly due to contacts with hydrophobic residues, whereas specific hydrogen bonds and π interactions were not identified. The ligand is completely buried in the p53-specific binding pocket of MDM2, in very good agreement with the homogeneous distribution of STD values observed in the binding epitope determined by NMR experiments (Figure 6).

When assembled all together, these data enable us to draw a preliminary picture of the impact of the ancillary ligands on the biological properties of the (C^N^{pz}^N)Au(III) complexes. First of all, complex **4** bearing the known anticancer agent 6-TG as the ancillary ligand seemed to possess cytotoxic properties very similar to those of its ligand. In that particular case, the biological properties may be due only to the ancillary ligand rather than to the Au(III) part. Complexes **1** and **3** were shown to have moderate activities. Indeed, both compounds appeared to be poorly taken up into A549 and MCF-7 cancer cells but were active against a potential intracellular target (i.e., MDM2−p53 or G4 and i-motif DNA structures for **1** or **3**, respectively).

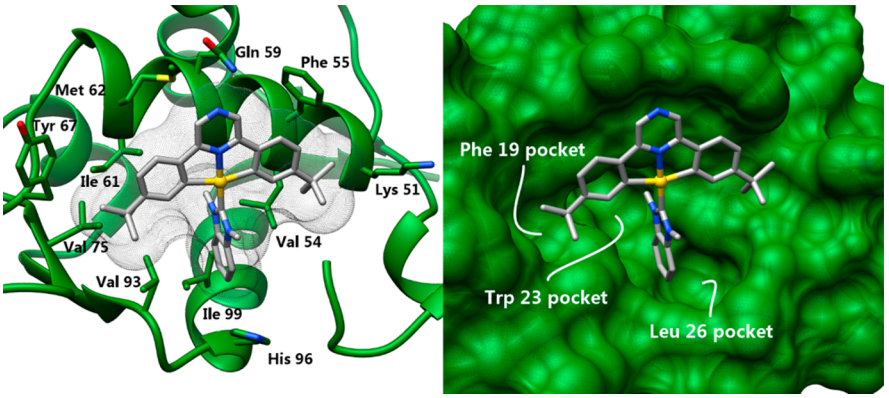

Figure 7. Representation of **2** (gray) docked in MDM2 (PDB entry 1T4E, green). On the left, the side chains of residues surrounding **2** (closer than 4 Å) are displayed. On the right, the surface of MDM2 and relevant pockets occupied by p53 residues are indicated.

DOI: 10.1021/acs.inorgchem.7b00339
Inorg. Chem. XXXX, XXX, XXX−XXX

This demonstrates the balance between uptake and reactivity that a drug candidate must fulfill in order to be active. Finally, complex **2**, which presented high cytotoxicity, fulfilled all of the requirements by being the most readily taken up into the cell and being active against all of the tested intracellular targets.

CONCLUSION

We have reported the synthesis and characterization of three new pyrazine-based cyclometalated (C^N^{pz}^C)Au(III) complexes. The crystal structure of one of these has been determined and revealed the typical slightly distorted square-planar geometry of cyclometalated (C^N^{pz}^C)Au(III) complexes. The antiproliferative screening of a series of seven cyclometalated (C^N^{pz}^C)Au(III) complexes, including the newly synthesized ones, on HL60 cells revealed compounds **1**−**4** as the most promising candidates. Compound **2** bearing a 1,3-dimethylbenzimidazol-2-ylidene ligand was shown to be the most active complex, with IC_{50} values down to nanomolar levels against cancer cells, although this was associated with comparatively high cytotoxicity against healthy fibroblasts. The uptake study using ICP-MS and fluorescence microscopy revealed that compound **2**, the most toxic complex, was present in A549 and MCF-7 cells at the highest concentrations. Compound **2** was shown by NMR spectroscopy to be highly stable toward GSH at room temperature over a time period of 6 days. Compound **2** also interacted more tightly with G-quadruplex DNA structures than its caffeine-based analogue **3**. Moreover, we have found the first evidence that gold complexes can stabilize i-motif DNA structures at both acidic and transitional pH values. We have also reported for the first time the inhibition of the MDM2−p53 interaction by gold-based complexes, which sheds new light on the possible intracellular targets of such cyclometalated complexes and might open the way for the optimization of new PPI inhibitors.

Overall, our study documents the importance of ancillary donor—here the NHC ligand—for the biological properties of cyclometalated Au(III) complexes. Benzimidazole-based NHC ligands appear to be particularly promising for the development of gold-based anticancer treatments. Further studies are ongoing to increase the selectivity of the complexes by targeting them to specific cancer cells.

EXPERIMENTAL SECTION

General Remarks. When required, manipulations were performed using standard Schlenk techniques under dry nitrogen or in an MBraun glovebox. Nitrogen was purified by passing it through columns of supported P_2O_5 with moisture indicator and activated 4 Å molecular sieves. Anhydrous solvents were freshly distilled from appropriate drying agents. ^{1}H and ^{13}C{^{1}H} spectra were recorded using a Bruker Avance DPX-300 spectrometer. ^{1}H NMR spectra (300.13 MHz) were referenced to the residual protons of the deuterated solvent used. ^{13}C{^{1}H} NMR spectra (75.47 MHz) were referenced internally to the D-coupled ^{13}C resonances of the NMR solvent. Elemental analyses were carried out at London Metropolitan University. UV−vis absorption spectra were recorded using a PerkinElmer Lambda 35 UV−vis spectrometer. Excitation and emission spectra were measured in a (TCSPC) Horiba Jobin Yvon FluoroLog spectrofluorometer. Compounds **1**, **5**, **6**, and **7** were synthesized following reported procedures.[19,20]

Synthesis and Characterization. *[(C^N^{pz}^N)Au(1,3-dimethylbenzimidazol-2-ylidene)]PF$_6$ (**2**).* A mixture of [(C^N^{pz}^N)AuCl (**1**) (50 mg, 0.087 mmol), 1,3-dimethylbenzimidazolium iodide (24 mg, 0.087 mmol), KO^{t}Bu (12 mg, 0.104 mmol), and KPF_6 (48 mg, 0.261 mmol) was stirred in distilled toluene (6 mL) at 80 °C overnight, leading to the formation of an orange precipitate. After the solution was cooled to room temperature, the solvent was evaporated, and the orange solid was dissolved in dichloromethane. The orange solution was filtered through Celite and concentrated under reduced pressure. Upon addition of light petroleum (bp 40−60 °C), an orange precipitate formed and was collected and dried to afford the pure product as an orange powder (54 mg, 0.065 mmol, 75% yield). Anal. Calcd for $C_{33}H_{36}N_4AuPF_6$ (830.2): C, 47.72; H, 4.37; N, 6.75. Found: C, 47.66; H, 4.48; N, 6.76. ^{1}H NMR (CD_2Cl_2, 300.13 MHz): δ 8.99 (s, 2H, H^2), 7.84 (m, 2H, H^{12}), 7.80 (d, $^3J_{H-H}$ = 8.2 Hz, 2H, H^5), 7.72 (m, 2H, H^{13}), 7.44 (dd, $^3J_{H-H}$ = 8.4 Hz, $^4J_{H-H}$ = 2.0 Hz, 2H, H^6), 6.98 (d, $^4J_{H-H}$ = 2.0 Hz, 2H, H^8), 4.16 (s, 6H, N−CH_3), 1.18 (s, 18H, ^{t}Bu). ^{13}C{^{1}H} NMR (CD_2Cl_2, 75.48 MHz): δ 165.3 (s, C^9), 162.5 (s, C^{10}), 158.0 (s, C$^{3/4}$), 157.3 (s, C$^{3/4}$), 145.0 (s, C^7), 139.8 (s, C^2), 134.6 (s, C^{11}), 133.3 (s, C^8), 127.3 (s, C^5), 126.6 (s, C^{13}), 125.9 (s, C^6), 112.5 (s, C^{12}), 36.5 (s, N−*Me*), 35.6 (s, C(*Me*)$_3$), 31.0 (s, C(*Me*)$_3$).

*[(C^N^{pz}^N)Au(1,3,7,9-tetramethylxanthin-8-ylidene)]BF$_4$ (**3**).* A mixture of **1** (50 mg, 0.087 mmol), 1,3,7,9-tetramethylxanthinium tetrafluoroborate (26 mg, 0.087 mmol), and KO^{t}Bu (12 mg, 0.104 mmol) was stirred in distilled toluene (7 mL) at 80 °C overnight, leading to the formation of an orange precipitate. After the solution was cooled to room temperature, the solvent was evaporated, and the orange solid was dissolved in dichloromethane. The orange solution was filtered through Celite and concentrated under reduced pressure. Upon addition of diethyl ether, a yellow precipitate formed and was collected, washed with water (3 × 3 mL), and dried to afford the pure product as a yellow powder (46 mg, 0.055 mmol, 67% yield). Anal. Calcd for $C_{33}H_{38}N_6O_2AuBF_6$ (834.3): C, 47.50; H, 4.59; N, 10.07. Found: C, 47.41; H, 4.50; N, 10.26. ^{1}H NMR (CD_2Cl_2, 300.13 MHz): δ 8.94 (s, 2H, H^2), 7.74 (d, $^3J_{H-H}$ = 8.2 Hz, 2H, H^5), 7.43 (dd, $^3J_{H-H}$ = 8.4 Hz, $^4J_{H-H}$ = 2.0 Hz, 2H, H^6), 7.20 (d, $^4J_{H-H}$ = 2.0 Hz, 2H, H^8), 4.29 (s, 3H, N−Me^{18}), 4.18 (s, 3H, N−Me^{11}), 3.93 (s, 3H, N−Me^{13}), 3.45 (s, 3H, N−Me^{15}), 1.18 (s, 18H, ^{t}Bu). ^{13}C{^{1}H} NMR (CD_2Cl_2, 75.48 MHz): δ 165.3 (s, C^9), 159.1 (s, C^{10}), 158.5 (s, C$^{3/4}$), 157.3 (s, C$^{3/4}$), 154.0 (s, C^{16}), 151.0 (s, C^{14}), 144.6 (s, C^7), 141.7 (s, C^{17}), 139.8 (s, C^2), 134.0 (s, C^8), 127.3 (s, C^5), 125.9 (s, C^6), 111.1 (s, C^{12}), 40.2 (s, N−*Me*^{18}), 38.7 (s, N−*Me*^{11}), 35.7 (s, *C*(Me)$_3$), 32.5 (s, N−*Me*^{13}), 31.0 (s, C(*Me*)$_3$), 29.03 (s, N−*Me*^{15}).

*(C^N^{pz}^N)Au(6-thioguanine) (**4**).* A mixture of **1** (50 mg, 0.087 mmol), K_2CO_3 (24 mg, 0.146 mmol), and 6-thioguanine (15 mg, 0.087 mmol) was stirred in a 1/1 acetone/MeOH mixture (10 mL) at room temperature for 3 h. The solution was evaporated to dryness, and the obtained orange solid was dissolved in the minimum amount of MeOH and diluted with DCM to a final volume of 20 mL. The solution was filtered over Celite and concentrated under vacuum. After addition of diethyl ether, an orange precipitate was obtained and filtered, washed with water (2 × 3 mL), and dried to afford the product with three waters of hydration as an orange powder (58 mg, 89% yield). Anal. Calcd for $C_{29}H_{30}N_7AuS{\cdot}3H_2O$ (759.7): C, 45.85; H, 4.78; N, 12.91. Found: C, 46.22; H, 4.32; N, 12.15. ^{1}H NMR (DMSO-d_6, 300.13 MHz): δ 9.24 (s, 2H, H^2), 8.32 (s, 1H, H^{10}), 7.88 (d, $^3J_{H-H}$ = 8.2 Hz, 2H, H^5), 7.57 (d, $^4J_{H-H}$ = 1.9 Hz, 2H, H^8), 7.32 (s, 1H, NH), 7.23 (dd, $^3J_{H-H}$ = 8.2 Hz, $^4J_{H-H}$ = 1.9 Hz, 2H, H^6), 5.11 (broad s, 2H, NH_2), 1.11 (s, 18H, ^{t}Bu). ^{13}C{^{1}H} NMR (DMSO-d_6, 75.48 MHz): 170.2 (s, C^9), 156.7 (s, C$^{3/4}$), 155.6 (s, C$^{3/4}$), 154.5 (s, C^7), 144.4 (s, C^{10}), 139.3 (s, C^2), 131.1 (s, C^8), 125.9 (s, C^5), 123.4 (s, C^6), 79.2 (s, C^{10}), 35.0 (s, *C*(CH$_3$)$_3$), 30.8 (s, *C*H$_3$).

X-ray Crystallography. A summary of the crystallographic information is collected in Table S1. Crystals of **2**·toluene were mounted on a MiTeGen MicroMesh and fixed in a cold nitrogen stream. Diffraction intensities were recorded at 140 K on a Rigaku HG Saturn724+ (2 × 2 bin mode) equipped with Mo Kα radiation. Data collection, refinement, and reduction were performed using the CrystalClear-SM Expert 3.1 b27 software, and the absorption correction was done at this stage.[63] Both structures were solved using SHELXT and refined by full-matrix least-squares methods on F^2 with SHELXL.[64] Non-hydrogen atoms were refined with anisotropic thermal parameters. Hydrogen atoms were included at idealized positions. No missed symmetry was reported by PLATON.[65] Computer programs used in this analysis were run through WinGX.[66] Scattering factors for neutral atoms were taken from the

DOI: 10.1021/acs.inorgchem.7b00339
Inorg. Chem. XXXX, XXX, XXX−XXX

literature.[67] In the structure of **2**·toluene, the PF_6^- anion showed statistic disorder that could not be modeled. For this reason, these atoms were restrained with effective standard deviation *s* so that their U_{ij} components approximate isotropic behavior. However, two large peaks of residual electron density close to the phosphorus atom with no chemical meaning were observed. This caused three A-alerts in the check-cif for this complex. CCDC 1521266 (**2**) contains the supplementary crystallographic data for this paper. These data can be obtained free of charge from The Cambridge Crystallographic Data Centre via www.ccdc.cam.ac.uk/data_request/cif.

Biological Testing. *Antiproliferation Assay.* Human HL60 and A549 cancer cell lines (from ECACC) were cultured in RPMI 1640 medium with 10% fetal calf serum, 2 mM L-glutamine, 100 units/mL penicillin, and 100 μg/mL streptomycin (Invitrogen). Cells were maintained in a humidified atmosphere at 37 °C and 5% CO_2. The human MCF-7 cancer cell line (from ECACC) and the human fetal fibroblast (MRC-5) cells were cultured in Dulbecco's modified Eagle's medium with 10% fetal calf serum, 2 mM L-glutamine, 100 units/mL penicillin, and 100 μg/mL streptomycin (Invitrogen). Cells were maintained in a humidified atmosphere at 37 °C with 5% CO_2. Inhibition of cancer cell proliferation was measured by the 3-(4,5-dimethylthiazol-2-yl)-5-(3-carboxymethoxyphenyl)-2-(4-sulfophenyl)-2*H*-tetrazolium (MTS) assay using the CellTiter 96 Aqueous One Solution Cell Proliferation Assay (Promega) and following the manufacturer's instructions. Briefly, cells (3×10^4/100 μL for HL60, 8×10^3/100 μL for both A549 and MCF-7, and 2×10^3/100 μL for MRC-5) were seeded in 96-well plates and left untreated or treated with 1 μL of DMSO (vehicle control) or 1 μL of complex diluted in DMSO at different concentrations in triplicate for 72 h at 37 °C with 5% CO_2. Following this, the MTS assay reagent was added for 4 h, and the absorbance measured at 490 nm using a Polarstar Optima microplate reader (BMG Labtech). IC_{50} values were calculated using GraphPad Prism version 5.0 software.

Uptake Study. A549 and MCF-7 cells were grown in 75 cm^2 flasks up to 70% of confluence in 10 mL of culture medium. Compounds **1**–**3** were added to the flasks (100 μL of 1 mM solution in DMSO) and incubated for 6 h at 37 °C with 5% CO_2. As negative controls, cells were incubated with DMSO alone under the same conditions. After removal of the medium and washing of the cells with phosphate-buffered saline (PBS) (pH 7.4), the cells were detached using a trypsin solution. After quenching of trypsin with fresh medium, centrifugation, and removal of the supernatant, the cell pellet was resuspended in 1 mL of PBS (pH 7.4) and split into two 500 μL aliquots for metal and protein quantification. The number of cells (expressed in millions of cells) in each sample was determined by measuring the protein content of the treated sample using a BCA assay (ThermoFischer Scientific) corrected by the amount of protein/10^6 cells, which was determined for each cell type by measuring the protein content of an untreated sample and dividing by the corresponding number of cells measured with a hematocytometer following a reported procedure.[68] Microwave digestion was used to solvate the samples to liquid form. Nitric acid and hydrogen peroxide were used in a Milestone Ethos 1 microwave system using an SK-10 10-place carousel. The digest was ramped to 200 °C in 15 min and held at 200 °C for 15 min. The sample was weighed into a microwave vessel before digestion and decanted and rinsed into a preweighed PFA bottle after digestion. ICP-MS samples were spiked with rhodium internal standard and run on a Thermo X series 1 ICP mass spectrometer. Isotopes selected were ^{63}Cu, ^{65}Cu, ^{107}Ag, ^{109}Ag, and ^{197}Au. Certified standards and an independent reference were used for accuracy. Acid blanks were run through the system and subtracted from sample measurements before corrections for dilution.

FRET Assay. The initial FRET melting screen was performed using a FRET DNA-melting-based assay. The sequences used were $hTeloC_{FRET}$ (5′-FAM-d[TAA-CCC-TAA-CCC-TAA-CCC-TAA-CCC]-TAMRA-3′; $hif\text{-}1\alpha_{FRET}$ (5′-d[CGC-GCT-CCC-GCC–CCC-TCT-CCC-CTC–CCC-GCG-C]-3′), $hTeloG_{FRET}$ (5′-FAM-d[GGG-TTA-GGG-TTA-GGG-TTA-GGG]-TAMRA-3′), and DS_{FRET} (5′-FAM-d[TAT-AGC-TAT-A-HEG(18)-TAT-AGC-TAT-A]-TAMRA-3′). The labeled oligonucleotides (the donor fluorophore, FAM, was 6-carboxyfluorescein; the acceptor fluorophore, TAMRA, was 6-carboxytetramethylrhodamine) were prepared as a 220 nM solution in 10 mM sodium cacodylate buffer at the indicated pH with 100 mM sodium chloride and then thermally annealed. Strip tubes (QIAgen) were prepared by aliquoting 18 μL of the annealed DNA followed by 2 μL of the compound solutions. Control samples for each run were prepared with the same quantity of DMSO with the DNA in buffer. Fluorescence melting curves were determined in a QIAgen Rotor-Gene Q-series PCR machine using a total reaction volume of 20 μL. Measurements were made with excitation at 470 nm and detection at 510 nm. Final analysis of the data was carried out using QIAgen Rotor-Gene Q-series software and Origin or Excel.

Fluorescence Polarization Assay. The fluorescence polarization assay was carried out on a BMG Labtech CLARIOstar microplate reader with a fluorescence polarization optic measuring at 490/520 nm. Black, flat-bottom, untreated polystyrene Corning 96-well black plates were used, and all of the reagents used in the assay were biological grade and purchased from Sigma-Aldrich, Novabiochem, or Thermo Fisher Scientific. All of the solutions were made using Milli-Q water. Samples and the positive control (wild-type p53, 4 mM) were dissolved in DMSO. Each well was prepared with 90 μL of a working solution of HDM2 (11.11 nM) and fluorescently tagged high-affinity peptide (FAM-LTFEHYWAQLTS-$CONH_2$, 11.11 nM) in PBS with 0.05% Tween-20 at pH 7.4. For the assay, 10 μL of either sample or positive or negative control was added to each well to obtain a final volume of 100 μL and 10 nM concentration of protein and tagged peptide. For screening purposes, the samples were tested in duplicate at a concentration of 100 μM. Compounds that showed inhibition were tested for IC_{50} using seven different concentrations in triplicate. The experiment was repeated to confirm the result. Each plate contained a positive control (wild-type p53, final concentration 400 μM) and a negative control (DMSO), both in triplicate. Before the plate was read, it was shaken manually to provide appropriate mixing and incubated at room temperature for 30 min, and the absence of bubbles was verified. Total fluorescence was also recorded to identify potential interference due to intrinsic fluorescence or quenching from the samples. Data analysis was performed with GraphPad Prism and Microsoft Excel. IC_{50} results were analyzed using nonlinear regression for the logarithm of the inhibitor versus response with variable slope.

NMR Spectroscopy. The NMR spectra were recorded at 25 °C in 25 mM PBS (pH 7.4), 1% DMSO-d_6 with D_2O as the solvent on an ultra-compact 800 MHz Bruker Avance III NMR spectrometer equipped with an inverse triple resonance (H/C/N) *z*-gradient probe head. For sample preparation, ligand **2** was lyophilized twice with 99% D_2O and once final in 99.99% D_2O from Sigma-Aldrich. Final concentrations were 13.5 μM MDM2 and 500 μM **2**. Chemical shift assignments for **2** were obtained at 800 MHz by means of COSY, TOCSY, NOESY (800 ms), and HSQC 2D NMR experiments. STD NMR experiments were carried out using a pseudo-2D pulse sequence including spoil pulses to destroy residual magnetization during the relaxation delay (two trim pulses of 2.5 and 5 ms followed by a 3 ms gradient pulse on the *Z* axis). For selective saturation of MDM2, cascades of 49 ms Gaussian-shaped pulses were used with a 1 ms delay between successive pulses. Total saturation times for STD measurements were 4 s (for binding detection) and 0.5 s (for binding epitope determination) on experiments consisting of 1024 scans. The short saturation time for the determination of the binding epitope avoids the introduction of artifacts due to different relaxation properties of protons of **2**. Selective saturation of the protein was achieved by setting the *on-resonance* frequency at 0 ppm in order to produce saturation of the aliphatic side chains of the protein. The irradiation frequency was shifted to 40 ppm for the reference (*off-resonance*) spectrum. The absence of direct irradiation of ligand ^1H signals was verified by blank STD NMR experiments (without protein). The binding epitope was determined by assigning 100% relative value to the most intense proton and normalizing the values of the remaining ligand protons against it.

Docking Calculations. Compound **2** was minimized using density functional theory with the B3LYP hybrid functional and the 6-311++G** basis set. For gold atoms, the LANL2DZ basis set and an

DOI: 10.1021/acs.inorgchem.7b00339
Inorg. Chem. XXXX, XXX, XXX–XXX

effective core potential (ECP) to treat the core electrons were used. Frequency calculations were performed to ensure that a stationary point was reached. Single-point calculations and population analysis were also performed using the TPSS functional[69] in combination with Grimme's D3 dispersion correction using Becke–Johnson damping.[70] The def2-TZVPP basis set was used.[71] All of the calculations were performed using Gaussian 09. Charge fitting was performed using the RESP fitting method provided by antechamber[72] with populations obtained from both functionals described above. The gold atom, which is not supported by the Autodock programs, was swapped with a dummy atom (C), and the ligand was then prepared for docking using AutoDockTools4.[73] MDM2 (PDB entry 1T4E) was prepared with UCSF Chimera[74] for protonation and subsequent relaxation of the hydrogens. A final step of preparation with AutoDockTools4[73] was necessary to convert the file to pdbqt format and introduce flexibility to the residues in the binding pocket: Gln 72, Met 62, Phe 55, Val 93, Ile 61, Ser 17, and Leu 54. Docking was performed with AutoDock 4.2.3[74] using a genetic algorithm (20 runs, medium evaluation), and the results were compared with NMR data to identify the binding pose (see NMR Spectroscopy). Replacing the gold atom with a dummy carbon atom is a simplification chosen after evaluation of the experimental results and with a specific aim. First, compound **2** is unlikely to interact with sulfur centers, as highlighted in Reaction of 2 with Glutathione, thus excluding a main interaction characteristic of some gold complexes. Second, from fluorescence polarization assays we identified displacement of the fluorescent probe from MDM2, which directed us to investigate the classic binding pocket of the protein. The pocket is rich in hydrophobic residues, and interactions with hydrophobic groups are a dominant motif in MDM2 binding, similarly to the natural substrate. The charge of the gold atom was determined at a quantum-mechanical level and assigned to the dummy atom, thus covering electrostatic contributions. Gold is fairly shielded by the methyl groups of the benzimidazole ligand and their orientation, thus minimizing the opportunity for direct contact. The method chosen allowed simple generation of a number of varied conformations and orientations of compound **2** in the binding pocket. Importantly, all of the generated poses were evaluated against NMR results independently by their docking scores, and the choice of the binding pose was based exclusively on experimental data, substantially nullifying the estimation factor related to the replacement of the gold atom with a dummy atom.

■ ASSOCIATED CONTENT

Supporting Information

The Supporting Information is available free of charge on the ACS Publications website at DOI: 10.1021/acs.inorgchem.7b00339.

Figures S1–S10 and Table S1 (PDF)

Crystallographic data for **2**·toluene (CIF)

■ AUTHOR INFORMATION

Corresponding Authors

*B.B.: Tel: +44 01680 1875. E-mail: b.bertrand@uea.ac.uk.

*M.O'C.: Tel: +44 016035 92030. E-mail: m.oconnell@uea.ac.uk.

*M.B.: Tel: +44 016035 92044. E-mail: m.bochmann@uea.ac.uk.

ORCID

Benoît Bertrand: 0000-0003-0542-4454

Manfred Bochmann: 0000-0001-7736-5428

Notes

The authors declare no competing financial interest.

■ ACKNOWLEDGMENTS

This work was supported by the European Research Council. M.B. is an ERC Advanced Investigator Award holder (Grant 338944-GOCAT). We are grateful to the EPSRC National Crystallographic Service (Southampton, U.K.) for collection of crystallographic data sets.[75] M.M.D.C. thanks the Research and Specialist Computing Support Service at the University of East Anglia for carrying out the calculations on the High Performance Computing Cluster.

■ REFERENCES

(1) Sun, H. Z.; Zhang, L.; Szeto, K. Y. Bismuth in medicine. *Met. Ions Biol. Syst.* **2004**, *41*, 333–378.

(2) Mjos, K. D.; Orvig, C. Metallodrugs in Medicinal Inorganic Chemistry. *Chem. Rev.* **2014**, *114*, 4540–4563.

(3) Rosenberg, B.; Van Camp, L.; Trosko, J. E.; Mansour, V. H. Platinum Compounds: a New Class of Potent Antitumour Agents. *Nature* **1969**, *222*, 385–386.

(4) (a) Bosl, G. J.; Bajorin, D. F.; Sheinfeld, J. *Cancer of the Testis*; DeVita, V. T. J., Hellman, S., Rosenberg, S. A., Eds.; Lippincott Williams & Wilkins: Philadelphia, 2001. (b) Watson, M.; Barrett, A.; Spence, R.; Twelves, C. *Oncology*, 2nd ed.; Oxford University Press: Oxford, U.K., 2006.

(5) (a) Rabik, C. A.; Dolan, M. E. Molecular mechanisms of resistance and toxicity associated with platinating agents. *Cancer Treat. Rev.* **2007**, *33*, 9–23. (b) Dilruba, S.; Kalayda, G. V. Platinum-based drugs: past, present and future. *Cancer Chemother. Pharmacol.* **2016**, *77*, 1103–1124. (c) Johnstone, T. C.; Suntharalingam, K.; Lippard, S. J. The Next Generation of Platinum Drugs: Targeted Pt(II) Agents, Nanoparticle Delivery, and Pt(IV) Prodrugs. *Chem. Rev.* **2016**, *116*, 3436–3486.

(6) Wheate, N. J.; Walker, S.; Craig, G. E.; Oun, R. The status of platinum anticancer drugs in the clinic and in clinical trials. *Dalton Trans.* **2010**, *39*, 8113–8127.

(7) Gasser, G.; Ott, I.; Metzler-Nolte, N. Organometallic Anticancer Compounds. *J. Med. Chem.* **2011**, *54*, 3–25.

(8) Hillard, E.; Vessières, A.; Thouin, L.; Jaouen, G.; Amatore, C. Ferrocene-Mediated Proton-Coupled Electron Transfer in a Series of Ferrocifen-Type Breast-Cancer Drug Candidates. *Angew. Chem., Int. Ed.* **2006**, *45*, 285–290.

(9) Santini, C.; Pellei, M.; Gandin, V.; Porchia, M.; Tisato, F.; Marzano, C. Advances in Copper Complexes as Anticancer Agents. *Chem. Rev.* **2014**, *114*, 815–862.

(10) Süss-Fink, G. Arene ruthenium complexes as anticancer agents. *Dalton Trans.* **2010**, *39*, 1673–1688.

(11) Ott, I. On the medicinal chemistry of gold complexes as anticancer drugs. *Coord. Chem. Rev.* **2009**, *253*, 1670–1681.

(12) (a) Berners-Price, S. J.; Filipovska, A. Gold compounds as therapeutic agents for human diseases. *Metallomics* **2011**, *3*, 863–873. (b) Gautier, A.; Cisnetti, F. Advances in metal–carbene complexes as potent anti-cancer agents. *Metallomics* **2012**, *4*, 23–32. (c) Zou, T. T.; Lum, C. T.; Lok, C. N.; Zhang, J. J.; Che, C. M. Chemical biology of anticancer gold(III) and gold(I) complexes. *Chem. Soc. Rev.* **2015**, *44*, 8786–8801. (d) Oehninger, L.; Rubbiani, R.; Ott, I. N-Heterocyclic carbene metal complexes in medicinal chemistry. *Dalton Trans.* **2013**, *42*, 3269–3284. (e) Liu, W. K.; Gust, R. Metal N-heterocyclic carbene complexes as potential antitumor metallodrugs. *Chem. Soc. Rev.* **2013**, *42*, 755–773. (f) Bertrand, B.; Casini, A. A golden future in medicinal inorganic chemistry: the promise of anticancer gold organometallic compounds. *Dalton Trans.* **2014**, *43*, 4209–4219. (g) Frik, M.; Fernandez-Gallardo, J.; Gonzalo, O.; Mangas-Sanjuan, V.; Gonzalez-Alvarez, M.; Serrano del Valle, A.; Hu, C.; Gonzalez-Alvarez, I.; Bermejo, M.; Marzo, I.; Contel, M. *J. Med. Chem.* **2015**, *58*, 5825–5841.

(13) Cutillas, N.; Yellol, G. S.; de Haro, C.; Vicente, C.; Rodriguez, V.; Ruiz, J. Anticancer cyclometalated complexes of platinum group metals and gold. *Coord. Chem. Rev.* **2013**, *257*, 2784–2797.

DOI: 10.1021/acs.inorgchem.7b00339
Inorg. Chem. XXXX, XXX, XXX–XXX

(14) Bertrand, B.; Spreckelmeyer, S.; Bodio, E.; Cocco, F.; Picquet, M.; Richard, P.; Le Gendre, P.; Orvig, C.; Cinellu, M. A.; Casini, A. Exploring the potential of gold(III) cyclometallated compounds as cytotoxic agents: variations on the C^N theme. *Dalton. Trans.* **2015**, *44*, 11911−11918.
(15) Sun, R. W.-Y.; Lok, C.-N.; Fong, T. T.-H.; Li, C. K.-L.; Yang, Z. F.; Zou, T.; Siu, A. F.-M.; Che, C.-M. A dinuclear cyclometalated gold(III)−phosphine complex targeting thioredoxin reductase inhibits hepatocellular carcinoma *in vivo*. *Chem. Sci.* **2013**, *4*, 1979−1988.
(16) Yan, J. J.; Chow, A. L.-F.; Leung, C.-H.; Sun, R. W.-Y.; Ma, D.-L.; Che, C.-M. Cyclometalated gold(III) complexes with N-heterocyclic carbene ligands as topoisomerase I poisons. *Chem. Commun.* **2010**, *46*, 3893−3895.
(17) Messori, L.; Orioli, P.; Tempi, C.; Marcon, G. Interactions of selected gold(III) complexes with calf thymus DNA. *Biochem. Biophys. Res. Commun.* **2001**, *281*, 352−360.
(18) Zhang, J.-J.; Sun, R. W.-Y.; Che, C.-M. A dual cytotoxic and anti-angiogenic water-soluble gold(III) complex induces endoplasmic reticulum damage in HeLa cells. *Chem. Commun.* **2012**, *48*, 3388−3390.
(19) Fernandez-Cestau, J.; Bertrand, B.; Blaya, M.; Jones, G. A.; Penfold, T. J.; Bochmann, M. Synthesis and Luminescence Modulation of Pyrazine-Based Gold(III) Pincer Complexes. *Chem. Commun.* **2015**, *51*, 16629−16632.
(20) Currie, L.; Fernandez-Cestau, J.; Rocchigiani, L.; Bertrand, B.; Lancaster, S. J.; Hughes, D. L.; Duckworth, H.; Jones, S. T. E.; Credgington, D.; Penfold, T. J.; Bochmann, M. Luminescent Gold(III) thiolates: Supramolecular interactions trigger and control switchable photoemissions from bimolecular excited states. *Chem. - Eur. J.* **2017**, *23*, 105−113.
(21) Zou, T.; Lum, C. T.; Lok, C.-N.; Zhang, J. J.; Che, C.-M. Chemical biology of anticancer gold(III) and gold(I) complexes. *Chem. Soc. Rev.* **2015**, *44*, 8786−8801.
(22) Zhu, Y.; Cameron, B. R.; Mosi, R.; Anastassov, V.; Cox, J.; Qin, L.; Santucci, Z.; Metz, M.; Skerlj, R. T.; Fricker, S. P. Inhibition of the cathepsin cysteine proteases B and K by square-planar cycloaurated gold(III) compounds and investigation of their anti-cancer activity. *J. Inorg. Biochem.* **2011**, *105*, 754−762.
(23) Mendes, F.; Groessl, M.; Nazarov, A. A.; Tsybin, Y. O.; Sava, G.; Santos, I.; Dyson, P. J.; Casini, A. Metal-Based Inhibition of Poly(ADP-ribose) Polymerase − The Guardian Angel of DNA. *J. Med. Chem.* **2011**, *54*, 2196−2206.
(24) Madeira, A.; de Almeida, A.; de Graaf, C.; Camps, M.; Zorzano, A.; Moura, T. F.; Casini, A.; Soveral, G. A Gold Coordination Compound as a Chemical Probe to Unravel Aquaporin-7 Function. *ChemBioChem* **2014**, *15*, 1487−1494.
(25) (a) Stefan, L.; Bertrand, B.; Richard, P.; Le Gendre, P.; Denat, F.; Picquet, M.; Monchaud, D. Assessing the differential affinity of small molecules for noncanonical DNA structures. *ChemBioChem* **2012**, *13*, 1905−1912. (b) Bertrand, B.; Stefan, L.; Pirrotta, M.; Monchaud, D.; Bodio, E.; Richard, P.; Le Gendre, P.; Warmerdam, E.; de Jager, M. H.; Groothuis, G. M. M.; Picquet, M.; Casini, A. Caffeine-Based Gold(I) *N*-Heterocyclic Carbenes as Possible Anticancer Agents: Synthesis and Biological Properties. *Inorg. Chem.* **2014**, *53*, 2296−2303. (c) Gratteri, P.; Massai, L.; Michelucci, E.; Rigo, R.; Messori, L.; Cinellu, M. A.; Musetti, C.; Sissi, C.; Bazzicalupi, C. Interactions of selected gold(III) complexes with DNA G-quadruplexes. *Dalton Trans.* **2015**, *44*, 3633−3639. (d) Bazzicalupi, C.; Ferraroni, M.; Papi, F.; Massai, L.; Bertrand, B.; Messori, L.; Gratteri, P.; Casini, A. Determinants for tight and selective binding of a medicinal dicarbene gold(I) complex to a telomeric DNA G-quadruplex: a joint ESI MS and XRD investigation. *Angew. Chem., Int. Ed.* **2016**, *55*, 4256−4259.
(26) Collie, G. W.; Parkinson, G. N. The application of DNA and RNA G-quadruplexes to therapeutic medicines. *Chem. Soc. Rev.* **2011**, *40*, 5867−5892.
(27) Biffi, G.; Tannahill, D.; McCafferty, J.; Balasubramanian, S. Quantitative visualization of DNA G-quadruplex structures in human cells. *Nat. Chem.* **2013**, *5*, 182−186.
(28) Monchaud, D.; Teulade-Fichou, M. P. A hitchhiker's guide to G-quadruplex ligands. *Org. Biomol. Chem.* **2008**, *6*, 627−636.
(29) Gehring, K.; Leroy, J. L.; Gueron, M. A tetrameric DNA structure with protonated cytosine.cytosine base pairs. *Nature* **1993**, *363*, 561−565.
(30) (a) Liu, D.; Balasubramanian, S. A Proton-Fuelled DNA Nanomachine. *Angew. Chem., Int. Ed.* **2003**, *42*, 5734−5736. (b) Day, H. A.; Wright, E. P.; Macdonald, C. J.; Gates, A. J.; Waller, Z. A. E. Reversible DNA i-motif to hairpin switching induced by copper(II) cations. *Chem. Commun.* **2015**, *51*, 14099−14102.
(31) Day, H. A.; Pavlou, P.; Waller, Z. A. E. i-Motif DNA: structure, stability and targeting with ligands. *Bioorg. Med. Chem.* **2014**, *22*, 4407−4418.
(32) Balasubramanian, S.; Hurley, L. H.; Neidle, S. Targeting G-quadruplexes in gene promoters: a novel anticancer strategy? *Nat. Rev. Drug Discovery* **2011**, *10*, 261−275.
(33) Debreczeni, J. E.; Bullock, A. N.; Atilla, G. E.; Williams, D. S.; Bregman, H.; Knapp, S.; Meggers, E. Ruthenium Half-Sandwich Complexes Bound to Protein Kinase Pim-1. *Angew. Chem., Int. Ed.* **2006**, *45*, 1580−1585.
(34) Feng, L.; Geisselbrecht, Y.; Blanck, S.; Wilbuer, A.; Atilla-Gokcumen, G. E.; Filippakopoulos, P.; Kräling, K. M.; Celik, A.; Harms, K.; Maksimoska, J.; Marmorstein, R.; Frenking, G.; Knapp, S.; Essen, L.-O.; Meggers, E. Structurally Sophisticated Octahedral Metal Complexes as Highly Selective Protein Kinase Inhibitors. *J. Am. Chem. Soc.* **2011**, *133*, 5976−5986.
(35) Pelay-Gimeno, M.; Glas, A.; Koch, O.; Grossmann, T. N. Structure-Based Design of Inhibitors of Protein-Protein Interactions: Mimicking Peptide Binding Epitopes. *Angew. Chem., Int. Ed.* **2015**, *54*, 8896−8927.
(36) Sheng, C.; Dong, G.; Miao, Z.; Zhang, W.; Wang, W. State-of-the-art strategies for targeting protein−protein interactions by small-molecule inhibitors. *Chem. Soc. Rev.* **2015**, *44*, 8238−828259.
(37) Leung, C.-H.; Zhong, H.-J.; Yang, H.; Cheng, Z.; Chan, D. S.-H.; Ma, V. P.-Y.; Abagyan, R.; Wong, C.-Y.; Ma, D.-L. A Metal-Based Inhibitor of Tumor Necrosis Factor-α. *Angew. Chem., Int. Ed.* **2012**, *51*, 9010−9014.
(38) Zhong, H.-J.; Lu, L.; Leung, K.-H.; Wong, C. C. L.; Peng, C.; Yan, S.-C.; Ma, D.-L.; Cai, Z.; Wang, H.-M. D.; Leung, C.-H. An iridium(III)-based irreversible protein−protein interaction inhibitor of BRD4 as a potent anticancer agent. *Chem. Sci.* **2015**, *6*, 5400−5408.
(39) Wade, M.; Li, Y.-C.; Wahl, G. M. MDM2, MDMX and p53 in oncogenesis and cancer therapy. *Nat. Rev. Cancer* **2013**, *13*, 83−96.
(40) Ortego, L.; Cardoso, F.; Martins, S.; Fillat, M. F.; Laguna, A.; Meireles, M.; Villacampa, M. D.; Gimeno, M. C. Strong inhibition of thioredoxin reductase by highly cytotoxic gold(I) complexes. DNA binding studies. *J. Inorg. Biochem.* **2014**, *130*, 32−37.
(41) Au, V. K.-M.; Wong, K. M.-C.; Zhu, N.; Yam, V. W.-W. Luminescent Cyclometalated *N*-Heterocyclic Carbene-Containing Organogold(III) Complexes: Synthesis, Characterization, Electrochemistry, and Photophysical Studies. *J. Am. Chem. Soc.* **2009**, *131*, 9076−9085.
(42) Bertrand, B.; Doulain, P.-E.; Goze, C.; Bodio, E. Development of trackable metal-based drugs: new generation of therapeutic agents. *Dalton Trans.* **2016**, *45*, 13005−13011.
(43) (a) Wang, D.; Xiang, D.-B.; Yang, X.-Q.; Chen, L.-S.; Li, M.-X.; Zhong, Z.-Y.; Zhang, Y.-S. APE1 overexpression is associated with cisplatin resistance in non-small cell lung cancer and targeted inhibition of APE1 enhances the activity of cisplatin in A549 cells. *Lung Cancer* **2009**, *66*, 298−304. (b) Michels, J.; Vitale, I.; Galluzzi, L.; Adam, J.; Olaussen, K. A.; Kepp, O.; Senovilla, L.; Talhaoui, I.; Guegan, J.; Enot, D. P.; Talbot, M.; Robin, A.; Girard, P.; Oréar, C.; Lissa, D.; Sukkurwala, A. Q.; Garcia, P.; Behnam-Motlagh, P.; Kohno, K.; Wu, G. S.; Brenner, C.; Dessen, P.; Saparbaev, M.; Soria, J.-C.; Castedo, M.; Kroemer, G. Cisplatin resistance associated with PARP hyperactivation. *Cancer Res.* **2013**, *73*, 2271−2280.
(44) Rubbiani, R.; Kitanovic, I.; Alborzinia, H.; Can, S.; Kitanovic, A.; Onambele, L. A.; Stefanopoulou, M.; Geldmacher, Y.; Sheldrick, W. S.; Wolber, G.; Prokop, A.; Wolfl, S.; Ott, I. Benzimidazol-2-ylidene

DOI: 10.1021/acs.inorgchem.7b00339
Inorg. Chem. XXXX, XXX, XXX−XXX

gold(I) complexes are thioredoxin reductase inhibitors with multiple antitumor properties. *J. Med. Chem.* **2010**, *53*, 8608−8618.
(45) Rubbiani, R.; Can, S.; Kitanovic, I.; Alborzinia, H.; Stefanopoulou, M.; Kokoschka, M.; Mönchgesang, S.; Sheldrick, W. S.; Wölfl, S.; Ott, I. Comparative in vitro evaluation of N-heterocyclic carbene gold(I) complexes of the benzimidazolylidene type. *J. Med. Chem.* **2011**, *54*, 8646−8657.
(46) Spreckelmeyer, S.; Orvig, C.; Casini, A. Cellular transport mechanisms of cytotoxic metallodrugs: an overview beyond cisplatin. *Molecules* **2014**, *19*, 15584−15610.
(47) Traverso, N.; Ricciarelli, R.; Nitti, M.; Marengo, B.; Furfaro, A. L.; Pronzato, M. A.; Marinari, U.M.; Domenicotti, C. Role of glutathione in cancer progression and chemoresistance. *Oxid. Med. Cell. Longevity* **2013**, *2013*, 972913.
(48) Chen, H. H. W.; Kuo, M. T. Role of Glutathione in the Regulation of Cisplatin Resistance in Cancer Chemotherapy. *Met.-Based Drugs* **2010**, *2010*, 430939.
(49) (a) Casini, A.; Cinellu, M. A.; Minghetti, G.; Gabbiani, C.; Coronnello, M.; Mini, E.; Messori, L. Structural and Solution Chemistry, Antiproliferative Effects, and DNA and Protein Binding Properties of a Series of Dinuclear Gold(III) Compounds with Bipyridyl Ligands. *J. Med. Chem.* **2006**, *49*, 5524−5531. (b) Zou, T.; Lum, C. T.; Chui, S. S.-Y.; Che, C.-M. Gold(III) complexes containing N-heterocyclic carbene ligands: thiol "switch-on" fluorescent probes and anti-cancer agents. *Angew. Chem., Int. Ed.* **2013**, *52*, 2930−2933.
(50) Pathak, R. K.; Dhar, S. Unique Use of Alkylation for Chemo-Redox Activity by a Pt(IV) Prodrug. *Chem. - Eur. J.* **2016**, *22*, 3029−3036.
(51) (a) Chen, Y.; Qu, K.; Zhao, C.; Wu, L.; Ren, J.; Wang, J.; Qu, X. Insights into the biomedical effects of carboxylated single-wall carbon nanotubes on telomerase and telomeres. *Nat. Commun.* **2012**, *3*, 1074. (b) Kang, H.-J.; Kendrick, S.; Hecht, S. M.; Hurley, L. H. The transcriptional complex between the BCL2 i-motif and hnRNP LL is a molecular switch for control of gene expression that can be modulated by small molecules. *J. Am. Chem. Soc.* **2014**, *136*, 4172−4185.
(52) Fung, S. K.; Zou, T.; Cao, B.; Lee, P.-Y.; Fung, Y. M. E.; Hu, D.; Lok, C.-N.; Che, C.-M. Cyclometalated gold(III) complexes containing N-heterocyclic carbene ligands engage multiple anti-cancer molecular targets. *Angew. Chem., Int. Ed.* **2017**, *56*, 3892−3896.
(53) (a) De Cian, A.; Guittat, L.; Kaiser, M.; Sacca, B.; Amrane, S.; Bourdoncle, A.; Alberti, P.; Teulade-Fichou, M. P.; Lacroix, L.; Mergny, J. L. Fluorescence-based melting assays for studying quadruplex ligands. *Methods* **2007**, *42*, 183−195. (b) Wright, E. P.; Day, H. A.; Ibrahim, A. M.; Kumar, J.; Boswell, L. J. E.; Huguin, C.; Stevenson, C. E. M.; Pors, K.; Waller, Z. A. E. Mitoxantrone and analogues bind and stabilize i-motif forming DNA sequences. *Sci. Rep.* **2016**, *6*, 39456.
(54) Phan, A. T.; Mergny, J.-L. Human telomeric DNA: G-quadruplex, i-motif and Watson-Crick double helix. *Nucleic Acids Res.* **2002**, *30*, 4618−4625.
(55) Brazier, J. A.; Shah, A.; Brown, G. D. I-motif formation in gene promoters: unusually stable formation in sequences complementary to known G-quadruplexes. *Chem. Commun.* **2012**, *48*, 10739−10741.
(56) Jia, L. Q.; Osada, M.; Ishioka, C.; Gamo, M.; Ikawa, S.; Suzuki, T.; Shimodaira, H.; Niitani, T.; Kudo, T.; Akiyama, M.; Kimura, N.; Matsuo, M.; Mizusawa, H.; Tanaka, N.; Koyama, H.; Namba, M.; Kanamaru, R.; Kuroki, T. Screening the p53 status of human cell lines using a yeast functional assay. *Mol. Carcinog.* **1997**, *19*, 243−253.
(57) Cominetti, M. M. D.; Goffin, S. A.; Raffel, E.; Turner, K. D.; Ramoutar, J. C.; O'Connell, M. A.; Howell, L. A.; Searcey, M. Identification of a new p53/MDM2 inhibitor motif inspired by studies of chlorofusin. *Bioorg. Med. Chem. Lett.* **2015**, *25*, 4878−4880.
(58) Mayer, M.; Meyer, B. Characterization of ligand binding by saturation transfer difference NMR spectroscopy. *Angew. Chem., Int. Ed.* **1999**, *38*, 1784−1788.
(59) Angulo, J.; Goffin, S. A.; Gandhi, D.; Searcey, M.; Howell, L. A. Unveiling the "Three Finger Pharmacophore" required for p53-MDM2 Inhibition by Saturation Transfer Difference NMR Initial Growth Rates Approach. *Chem. - Eur. J.* **2016**, *22*, 5858−5862.
(60) Blume, A.; Angulo, J.; Biet, T.; Peters, H.; Benie, A. J.; Palcic, M.; Peters, T. Fragment-based Screening of the Donor Substrate Specificity of Human Blood Group B Galactosyltransferase Using Saturation Transfer Difference NMR. *J. Biol. Chem.* **2006**, *281*, 32728−32740.
(61) (a) Kussie, P. H.; Gorina, S.; Marechal, V.; Elenbaas, B.; Moreau, J.; Levine, A. J.; Pavletich, N. P. Structure of the MDM2 Oncoprotein Bound to the p53 Tumor Suppressor Transactivation Domain. *Science* **1996**, *274*, 948−953. (b) Böttger, A.; Böttger, V.; Garcia-Echeverria, C.; Chène, P.; Hochkeppel, H. K.; Sampson, W.; Ang, K.; Howard, S. F.; Picksley, S. M.; Lane, D. P. Molecular characterization of the hdm2-p53 interaction. *J. Mol. Biol.* **1997**, *269*, 744−756.
(62) Zhao, Y.; Aguilar, A.; Bernard, D.; Wang, S. Small-Molecule Inhibitors of the MDM2−p53 Protein−Protein Interaction (MDM2 Inhibitors) in Clinical Trials for Cancer Treatment. *J. Med. Chem.* **2015**, *58*, 1038−1052.
(63) *CrysAlisPro*; Oxford Diffraction Ltd.: Abingdon, U.K., 2010.
(64) Sheldrick, G. M. A short history of *SHELX*. *Acta Crystallogr., Sect. A: Found. Crystallogr.* **2008**, *64*, 112−122.
(65) (a) Spek, A. L. *PLATON: A Multipurpose Crystallographic Tool*; Utrecht University: Utrecht, The Netherlands, 2006. (b) Spek, A. L. PLATON, An Integrated Tool for the Analysis of the Results of a Single Crystal Structure Determination. *Acta Crystallogr., Sect. A: Found. Adv.* **1990**, *46*, C34.
(66) Farrugia, L. J. *WinGX* suite for small-molecule single-crystal crystallography. *J. Appl. Crystallogr.* **1999**, *32*, 837−838.
(67) *International Tables for X-ray Crystallography*; Kluwer Academic Publishers: Dordrecht, The Netherlands, 1992; Vol. *C*, pp 500, 219, and 193.
(68) Wenzel, M.; Bertrand, B.; Eymin, M.-J.; Comte, V.; Harvey, J. A.; Richard, P.; Groessl, M.; Zava, O.; Amrouche, H.; Harvey, P. D.; Le Gendre, P.; Picquet, M.; Casini, A. Multinuclear cytotoxic metallodrugs: physico-chemical characterization and biological properties of novel heteronuclear gold-titanium complexes. *Inorg. Chem.* **2011**, *50*, 9472−9480.
(69) Tao, J.; Perdew, J. P.; Staroverov, V. N.; Scuseria, G. E. Climbing the Density Functional Ladder: Nonempirical Meta-Generalized Gradient Approximation Designed for Molecules and Solids. *Phys. Rev. Lett.* **2003**, *91*, 146401.
(70) (a) Grimme, S.; Antony, J.; Ehrlich, S.; Krieg, H. A consistent and accurate ab initio parametrization of density functional dispersion correction (DFT-D) for the 94 elements H-Pu. *J. Chem. Phys.* **2010**, *132*, 154104. (b) Grimme, S.; Ehrlich, S.; Goerigk, L. Effect of the damping function in dispersion corrected density functional theory. *J. Comput. Chem.* **2011**, *32*, 1456−1465.
(71) (a) Weigend, F.; Ahlrichs, R. Balanced basis sets of split valence, triple zeta valence and quadruple zeta valence quality for H to Rn: Design and assessment of accuracy. *Phys. Chem. Chem. Phys.* **2005**, *7*, 3297−3305. (b) Weigend, F. Accurate Coulomb-fitting basis sets for H to Rn. *Phys. Chem. Chem. Phys.* **2006**, *8*, 1057−1065.
(72) Case, D. A.; Darden, T. A.; Cheatham, T. E., III; Simmerling, C. L.; Wang, J.; Duke, R. E.; Luo, R.; Walker, R. C.; Zhang, W.; Merz, K. M.; Roberts, B.; Hayik, S.; Roitberg, A.; Seabra, G.; Swails, J.; Götz, A. W.; Kolossváry, I.; Wong, K. F.; Paesani, F.; Vanicek, J.; Wolf, R. M.; Liu, J.; Wu, X.; Brozell, S. R.; Steinbrecher, T.; Gohlke, H.; Cai, Q.; Ye, X.; Wang, J.; Hsieh, M.-J.; Cui, G.; Roe, D. R.; Mathews, D. H.; Seetin, M. G.; Salomon-Ferrer, R.; Sagui, C.; Babin, V.; Luchko, T.; Gusarov, S.; Kovalenko, A.; Kollman, P. A. *AMBER 12*; University of California: San Francisco, 2012.
(73) Morris, G. M.; Huey, R.; Lindstrom, W.; Sanner, M. F.; Belew, R. K.; Goodsell, D. S.; Olson, A. J. AutoDock4 and AutoDockTools4: Automated docking with selective receptor flexibility. *J. Comput. Chem.* **2009**, *30*, 2785−2791.
(74) Pettersen, E. F.; Goddard, T. D.; Huang, C. C.; Couch, G. S.; Greenblatt, D. M.; Meng, E. C.; Ferrin, T. E. UCSF Chimera—A visualization system for exploratory research and analysis. *J. Comput. Chem.* **2004**, *25*, 1605−1612.

DOI: 10.1021/acs.inorgchem.7b00339
Inorg. Chem. XXXX, XXX, XXX−XXX

(75) Coles, S. J.; Gale, P. A. Changing and Challenging Times for Service Crystallography. *Chem. Sci.* **2012**, *3*, 683−689.

DOI: 10.1021/acs.inorgchem.7b00339
Inorg. Chem. XXXX, XXX, XXX−XXX